

A General Neural Backbone for Mixed-Integer Linear Optimization via Dual Attention

Peixin Huang^{1†}, Yaxin Wu^{2†}, Yining Ma³, Cathy Wu³,
Wen Song^{1*}, Wei Zhang^{1*}

¹Shandong University, No. 72, Binhai Road, Qingdao, 266237, Shandong, China.

²Eindhoven University of Technology, De Zaale, Eindhoven, 513 5600 MB, Netherlands.

³Massachusetts Institute of Technology, 77 Massachusetts Avenue, Cambridge, 02139, Massachusetts, USA.

*Corresponding author(s). E-mail(s): wensong@email.sdu.edu.cn;
davidzhang@sdu.edu.cn;

Contributing authors: peixinhuang@mail.sdu.edu.cn; y.wu2@tue.nl;
yiningma@mit.edu; cathywu@mit.edu;

†These authors contributed equally to this work.

Abstract

Mixed-integer linear programming (MILP), a widely used modeling framework for combinatorial optimization, are central to many scientific and engineering applications, yet remains computationally challenging at scale. Recent advances in deep learning address this challenge by representing MILP instances as variable-constraint bipartite graphs and applying graph neural networks (GNNs) to extract latent structural patterns and enhance solver efficiency. However, this architecture is inherently limited by the local-oriented mechanism, leading to restricted representation power and hindering neural approaches for MILP. Here we present an attention-driven neural architecture that learns expressive representations beyond the pure graph view. A dual-attention mechanism is designed to perform parallel self- and cross-attention over variables and constraints, enabling global information exchange and deeper representation learning. We apply this general backbone to various downstream tasks at the instance level, element level, and solving state level. Extensive experiments across widely used

benchmarks show consistent improvements of our approach over state-of-the-art baselines, highlighting attention-based neural architectures as a powerful foundation for learning-enhanced mixed-integer linear optimization.

Keywords: General Combinatorial Optimization, Mixed-Integer Linear Programming, Deep Learning, Attention Mechanism

1 Introduction

Combinatorial Optimization Problems (COPs) are ubiquitous in science and engineering [1–5]. However, a major computational bottleneck for COP solving is the well-known NP-hardness, making it very challenging to solve large-scale problems in practice. The recent surge of Neural Combinatorial Optimization (NCO) has become a promising direction to break through this scalability bottleneck [6]. Based on historical data, NCO methods leverage deep (reinforcement) learning to discover useful hidden patterns through offline learning, so as to achieve fast online solving and overcome the efficiency and optimality limitation of human-designed algorithmic framework or components. Among NCO studies, research on *general* COP models is of particular importance due to their wide applicability in modeling various problems and the availability of off-the-shelf solvers with robust performance and optimality guarantee.

In this paper, we focus on Mixed-Integer Linear Programming (MILP), the workhorse of combinatorial optimization in practice [6, 7]. Though MILP does not cover the full spectrum of COP, it is general enough to model a large portion of scientific and engineering problems across various domains such as manufacturing [8], logistics [9], finance [10], biology [11], medicine [12], and chemistry [13]. Due to its strong application value, MILP has been a long-standing pillar of mathematical optimization, with very active research communities and strong general-purpose solvers such as Gurobi, CPLEX, and SCIP [14]. While performance of these modern MILP solvers has been continuously improved during the past decades, efficiently solving large-scale practical problems remains extremely challenging due to the strong NP-hardness. Motivated by the recent success of NCO, deep learning has been applied in various ways to speed up MILP solvers [15], such as learning primal heuristics to find high-quality feasible solution quickly [16–24], learning branching heuristics to reduce search tree size [25–32], learning cutting plane control policies to speed up linear programming solving at each node [33–37].

While deep learning for MILP is thriving, research on the backbone neural architecture is surprisingly sparse, which is the key bottleneck in this emerging field. As the foundation of learning based MILP models, the backbone neural architecture is responsible for extracting high-level feature embeddings from raw instance data to facilitate downstream learning tasks. The mainstream and state-of-the-art approach is to model MILP instance as a variable-constraint bipartite graph, and apply Graph Neural Network (GNN) to extract variable and constraint embeddings through message passing and aggregation among neighboring nodes [25, 38]. This neural architecture encodes

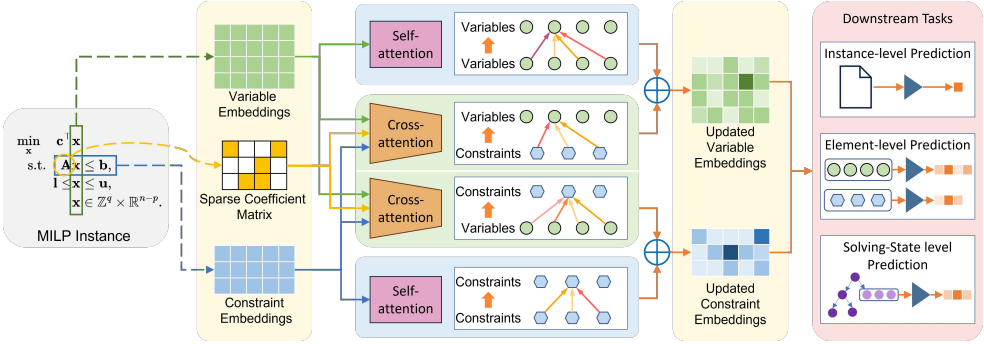


Fig. 1: Overview of the proposed attention-driven architecture.

the structural information of MILP through local message passing and is naturally size-invariant, and is able to handle instances of varying scales.

However, the above graph-based scheme has limited power in MILP representation, mainly due to its local-oriented mechanism. Specifically, in one layer of GNN, each node can only fuse information within its one-hop neighborhood, resulting in a very limited receptive field. Stacking multiple GNN layers cannot effectively alleviate this bottleneck because node embeddings quickly become indistinguishable due to GNN's inherent over-smoothing and over-squashing issues [39, 40]. The consequence is that each node's information source is within a small local range (normally within 4 hops in the bipartite graph), which significantly impairs the capability of graph-based architectures in capturing deeper representations and long-range dependencies that is crucial for efficiently solving general COPs. The limited expressive power of GNN in representing MILP has been noticed and theoretically studied in several works [41–43]. However, they are still under the local-oriented framework of GNN, and essentially cannot overcome this limitation.

This paper addresses the fundamental challenge of designing a more powerful backbone representation learning architecture for MILP, the most widely adopted modeling framework for COPs in practice. Different from existing works, we propose to view an MILP instance as two types of heterogeneous elements, i.e., variables and constraints. Then, we design a novel neural architecture to extract element embeddings through a dual-attention mechanism, as illustrated in Fig. 1. The first aspect is to analyze the intra-type relationships through full self-attention, enabling each node to directly access information from any other node of the same type. The second aspect is to capture inter-type relationships through bidirectional cross-attention, so as to exploit variable-constraint dependencies inherent in the MILP instance's structure. With this design, each element can globally establish direct and adaptive connections with long-range ones, significantly enhancing its receptive field. Moreover, more layers can be stacked to enhance the quality of generated embeddings, thereby overcoming limitations of existing graph-based architectures.

Through this paradigm, we aim to establish a new foundation for deep learning-based general combinatorial optimization solving. Our architecture serves as a general backbone that can be readily applied to diverse MILP learning tasks, including

instance-level prediction (e.g., feasibility and optimal objective), element-level prediction (e.g., optimal solution), and solving state-level prediction (e.g., branching policy). Extensive experiments on problems from various domains demonstrate that the proposed attention-based architecture exhibits substantially stronger expressive power than existing GNN counterparts, suggesting that attention-driven representations may constitute a new paradigm for learning to solve general COPs.

2 Preliminaries

Mixed-Integer Linear Programming (MILP). A general MILP with n variables and m constraints can be formally defined as

$$\min \mathbf{c}^\top \mathbf{x}, \quad \text{s.t.} \quad \mathbf{Ax} \leq \mathbf{b}, \quad \mathbf{l} \leq \mathbf{x} \leq \mathbf{u}, \quad \mathbf{x} \in \mathbb{Z}^q \times \mathbb{R}^{n-p}, \quad (1)$$

where \mathbf{x} is a vector of n decision variables, with q of them being integer variables and the rest $n - q$ variables being continuous. $\mathbf{c} \in \mathbb{R}^n$ represents the coefficient of each variable in the objective function. $\mathbf{A} \in \mathbb{R}^{m \times n}$ is the coefficient matrix of the m constraints, and $\mathbf{b} \in \mathbb{R}^m$ is the corresponding right-hand side values. $\mathbf{l} \in (\mathbb{R} \cup \{-\infty\})^n$ and $\mathbf{u} \in (\mathbb{R} \cup \{+\infty\})^n$ denote the upper and lower bound for each variable, respectively. MILP is very general and broadly applicable to many COPs.

Graph-based MILP Representation. The key of learning-based MILP solving is to extract *embeddings* of variables to enable downstream learning tasks such as instance feasibility prediction and optimal solution prediction. To this end, Gasse et al. [25] proposed a two-stage GNN that has become the de facto architecture for MILP representation learning. It models an MILP instance as a bipartite graph $\mathcal{G} = (\mathcal{V}, \mathcal{C}, \mathcal{E})$, where $\mathcal{V} = \{v_1, v_2, \dots, v_n\}$ is the variable node set with v_i representing i -th variable, $\mathcal{C} = \{c_1, c_2, \dots, c_m\}$ is the constraint node set with c_j representing the j -th constraint, and $\mathcal{E} = \{e_{ij} | \mathbf{A}_{ij} \neq 0, \forall 1 \leq i \leq n, 1 \leq j \leq m\}$ is the edge set with e_{ij} representing a nonzero constraint coefficient in the MILP instance. Let $\mathbf{B} \in \{0, 1\}^{n \times m}$ be the bipartite adjacency matrix with $\mathbf{B}_{ij} = 1$ if $e_{ij} \in E$. Each element $v_i \in \mathcal{V}$, $c_i \in \mathcal{C}$ and $e_{ij} \in \mathcal{E}$ is equipped with a raw feature vector $h_i^V \in \mathbf{H}_0^V$, $h_j^C \in \mathbf{H}_0^C$ and $h_{ij}^E \in \mathbf{H}_0^E$ to describe numerical and structural information of the MILP instance (listed in Appendix A). These raw features are first mapped to a d -dimensional space, and then pass through a two-stage bipartite GNN (BGNN) process:

$$\mathbf{H}^C \leftarrow \text{MLP}^C(\mathbf{H}^C, (\mathbf{B}^\top \mathbf{H}^V, \mathbf{H}^E)), \quad \mathbf{H}^V \leftarrow \text{MLP}^V(\mathbf{H}^V, (\mathbf{B} \mathbf{H}^C, \mathbf{H}^E)) \quad (2)$$

where $\mathbf{H}^C = \text{MLP}_0^V(\mathbf{H}_0^V) \in \mathbb{R}^{m \times d}$ and $\mathbf{H}^V = \text{MLP}_0^V(\mathbf{H}_0^C) \in \mathbb{R}^{n \times d}$ denote the embeddings of constraints and variables, $\mathbf{H}^E = \mathbf{H}_0^E W_0^E \in \mathbb{R}^{e \times d}$ denotes edge feature embeddings, MLP_0^V , MLP_0^C , MLP^C and MLP^V are two multi-layer perceptrons with ReLU activation, W_0^E is a learnable parameter. Essentially, each constraint first receives messages from its immediate variables to update its own embedding, and then each variable performs similar operations considering its immediate constraints.

In this graph-based scheme, message passing occurs only within the one-hop neighborhood of each variable or constraint node. In principle, accessing information from

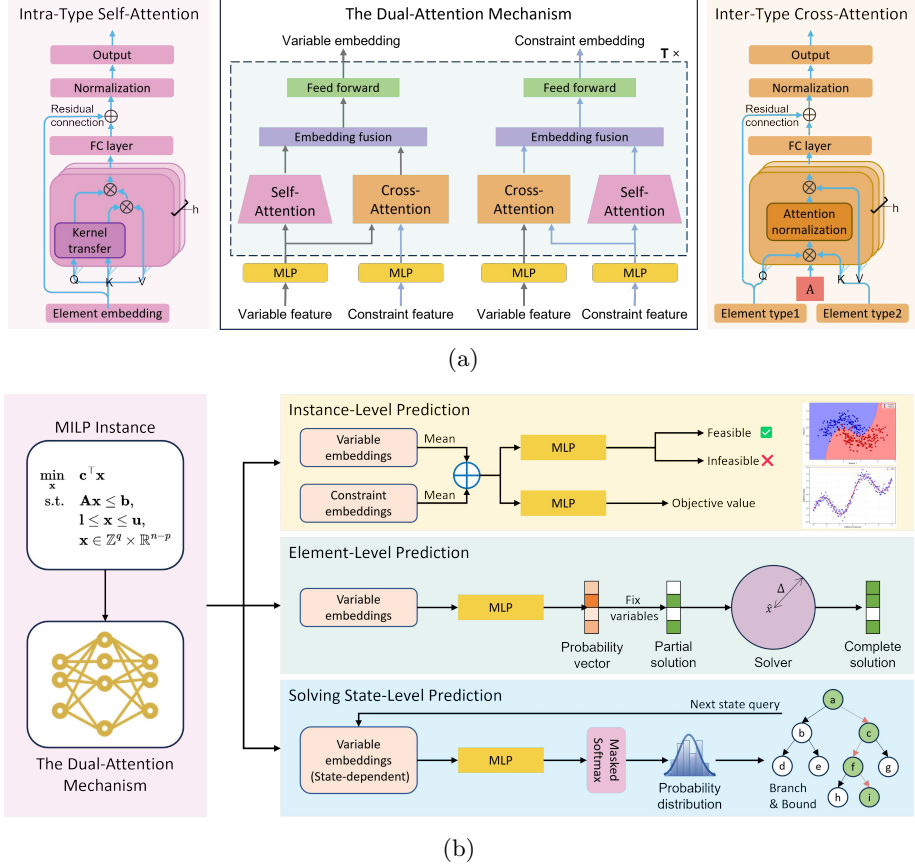


Fig. 2: Model Architecture and applications in downstream tasks. (a) The dual-attention mechanism (middle panel) consists of two intra-type self-attention modules (left panel) and two inter-type cross-attention modules (right panel) that work collectively in parallel to extract variable and constraint embeddings. (b) Applying our model to three distinct tasks on instance level (predicting instance feasibility and optimal objective value), element level (predicting values of binary variables), and solving state level (predicting the variable to branch at each B&B node).

a node that is k hops away requires k rounds of message passing, i.e., $\lceil k/2 \rceil$ layers BGNN. However, this is impractical for long-range nodes because the discriminative power of BGNN rapidly deteriorates with the increase of layers (which will be demonstrated in the experiments). Consequently, most existing works employ only 1 or 2 GNN layers. This inherent limitation restricts the model’s ability to extract deeper representations and capture long-range dependencies between variable and constraint nodes.

3 Method

In this paper, we go beyond the pure graph view of MILP, by considering variables and constraints as two types of key elements in MILP of equal importance. Building upon this element-centric view, we propose an attention-driven architecture to extract high-quality element embeddings through intra-type and inter-type relational learning. As shown in Fig. 2a, our model is a stack of T identical layers with independent trainable parameters. In each layer $t \in \{1, \dots, T\}$, the element embeddings are processed by a dual-attention mechanism to get updated embeddings \mathbf{H}_t^V and \mathbf{H}_t^C for the variables and constraints. This mechanism will be further detailed in the next subsection.

3.1 The Dual-Attention Mechanism

The motivation behind the dual-attention mechanism is to overcome the locality limitation of conventional GNN-based models. While message passing in BGNNs is limited to one-hop neighborhoods, we use attention mechanisms to enable each node to directly interact with any other node, thereby facilitating global information exchange. In our design, the dual-attention mechanism consists of two complementary components: self-attention and cross-attention. The self-attention modules are applied separately to the variable set and constraint set, allowing each node to aggregate information from all other nodes of the same type. In contrast, the cross-attention module models interactions between variables and constraints, enabling the network to reason about the structural patterns of the MILP instance. Through iterative stacking of multiple dual-attention layers, the architecture effectively captures deeper representations with both global and local dependencies, providing a more expressive representation of the MILP structure than traditional message-passing networks.

Intra-Type Self-Attention. In this part, we utilize the self-attention mechanism [44] on the variable set \mathcal{V} and constraint set \mathcal{C} to extract the corresponding embeddings. For the n variables, we first compute the query/key/value matrices as with $\mathbf{Q}_V = \mathbf{H}_{t-1}^V W_Q^V$, $\mathbf{K}_V = \mathbf{H}_{t-1}^V W_K^V$, and $\mathbf{V}_V = \mathbf{H}_{t-1}^V W_V^V$, where W_Q^V , W_K^V , W_V^V are trainable parameters. Then, the variable embeddings are updated as follows:

$$\mathbf{H}_{\text{self},t}^V = \text{SelfAttn}_V(\mathbf{Q}_V, \mathbf{K}_V, \mathbf{V}_V) = \text{softmax}\left(\frac{\mathbf{Q}_V \mathbf{K}_V^\top}{\sqrt{d}}\right) \mathbf{V}_V. \quad (3)$$

The constraint embeddings are computed similarly as:

$$\mathbf{H}_{\text{self},t}^C = \text{SelfAttn}_C(\mathbf{Q}_C, \mathbf{K}_C, \mathbf{V}_C) = \text{softmax}\left(\frac{\mathbf{Q}_C \mathbf{K}_C^\top}{\sqrt{d}}\right) \mathbf{V}_C, \quad (4)$$

where $\mathbf{Q}_C = \mathbf{H}_{t-1}^C W_Q^C$, $\mathbf{K}_C = \mathbf{H}_{t-1}^C W_K^C$, and $\mathbf{V}_C = \mathbf{H}_{t-1}^C W_V^C$. This step allows all variable (or constraint) nodes to exchange information globally within the same type, regardless of their distance in the bipartite graph.

Self-attention is known to be heavy. Assuming $d \ll n$, the time and memory complexity of the above procedure are $O(n^2d + m^2d)$ and $O(n^2 + m^2)$ respectively, which forms a major bottleneck in practice considering that large-scale MILP instance

could have more than 10000 variables and constraints. To address this issue, we employ a simple kernel trick [45] to linearize and approximate the standard self-attention function as follows:

$$\tilde{\mathbf{H}}_{\text{self},t}^V = \frac{\sigma(\mathbf{Q}_V)(\sigma(\mathbf{K}_V^\top)\mathbf{V}_V)}{\sigma(\mathbf{Q}_V)\sum_i \sigma(\mathbf{K}_V^\top(i,:)) + \epsilon} \approx \mathbf{H}_{\text{self},t}^V, \quad (5)$$

$$\tilde{\mathbf{H}}_{\text{self},t}^C = \frac{\sigma(\mathbf{Q}_C)(\sigma(\mathbf{K}_C^\top)\mathbf{V}_C)}{\sigma(\mathbf{Q}_C)\sum_j \sigma(\mathbf{K}_C^\top(j,:)) + \epsilon} \approx \mathbf{H}_{\text{self},t}^C, \quad (6)$$

where σ denotes the sigmoid function to guarantee the attention scores are positive and ϵ is a small non-zero positive number (set to $1e-8$) used to prevent zero denominator. By first computing $\sigma(\mathbf{K}_V^\top)\mathbf{V}_V$ and $\sigma(\mathbf{K}_C^\top)\mathbf{V}_C$ in Eq. (5) and (6), the time complexity is reduced to $O(nd^2 + md^2)$. The initial calculation of $\sigma(\mathbf{K}^\top)\mathbf{V}$ occupies memory space $O(d^2)$ and $\sigma(\mathbf{Q})$ multiplied by the pre-computed result of $\sigma(\mathbf{K}^\top)\mathbf{V}$ occupies $O(nd)$ or $O(md)$ memory. Thus, the overall memory complexity is reduced to $O((n + m)d)$.

We use H attention heads to enhance the representation power. These outputs subsequently undergo a residual connection and layer normalization to get the final embeddings as follows:

$$\mathbf{H}_{\text{self},t}^V = \text{LayerNorm} \left(\mathbf{H}_{t-1}^V + \left(\parallel_{h=1}^H \tilde{\mathbf{H}}_{\text{self},t,h}^V \right) \mathbf{W}_t^V \right), \quad (7)$$

$$\mathbf{H}_{\text{self},t}^C = \text{LayerNorm} \left(\mathbf{H}_{t-1}^C + \left(\parallel_{h=1}^H \tilde{\mathbf{H}}_{\text{self},t,h}^C \right) \mathbf{W}_t^C \right). \quad (8)$$

where \parallel denotes concatenation, \mathbf{W}_t^V and \mathbf{W}_t^C are trainable parameter used to map the Hd -dimensional feature back to d .

Inter-Type Cross-Attention. We consider variables and constraints are of equal importance, and design a bidirectional cross-attention mechanism to analyze the relationship between the two types of elements. For the variables, we compute the query matrix $\mathbf{Q}_V = \mathbf{H}_{t-1}^V W_Q^V$ using variable embeddings, and compute the key/value matrices $\mathbf{K}_C = \mathbf{H}_{t-1}^C W_K^C$ and $\mathbf{V}_C = \mathbf{H}_{t-1}^C W_V^C$ using constraint embeddings, where W_Q^V, W_K^C, W_V^C are trainable parameters¹. The variable embeddings are then updated as follows:

$$\mathbf{H}_{\text{cross},t}^V = \text{CrossAttn}_V(\mathbf{Q}_V, \mathbf{K}_C, \mathbf{V}_C) = \text{softmax} \left(\frac{\mathbf{Q}_V \mathbf{K}_C^\top}{\sqrt{d}} \right) \mathbf{V}_C. \quad (9)$$

The constraint embeddings can be computed in the same fashion:

$$\mathbf{H}_{\text{cross},t}^C = \text{CrossAttn}_C(\mathbf{Q}_C, \mathbf{K}_V, \mathbf{V}_V) = \text{softmax} \left(\frac{\mathbf{Q}_C \mathbf{K}_V^\top}{\sqrt{d}} \right) \mathbf{V}_V, \quad (10)$$

where $\mathbf{Q}_C = \mathbf{H}_{t-1}^C W_Q^C$, $\mathbf{K}_V = \mathbf{H}_{t-1}^V W_K^V$, and $\mathbf{V}_V = \mathbf{H}_{t-1}^V W_V^V$.

¹The trainable parameters of the cross-attention module differ from those of the self-attention module. For notational simplicity, we omit the explicit dependence on the module.

The above cross-attention implementation has two weaknesses. First, the structural information of the MILP instance is not explicitly considered. Second, since each element needs to exchange information from all nodes of the other type, the time and memory complexities are $O(mnd)$ and $O(mn)$ respectively, rendering it too expensive to large-scale MILP instances. To address this issue, we incorporate the coefficient matrix \mathbf{A} in the MILP problem into the cross-attention computation. As is well known, \mathbf{A} is often sparse, which can be exploited to obtain structural properties and speed up computation. Specifically, for the variable-to-constraint attention, we compute a sparse and MILP coefficient-aware attention score matrix \mathbf{M}_V , where $\mathbf{M}_{V,ij} = \exp(p_{ij})$ is the attention score from variable i to constraint j and $p_{ij} = \sum_{k=1}^d \frac{[\mathbf{Q}_{V,i} \odot \mathbf{K}_{C,j}]}{\sqrt{d}} \odot (\mathbf{W}_{E,ij} \mathbf{A}_{ij})_k$, where $\mathbf{W}_{E,ij}$ is trainable parameter. Clearly, $\mathbf{M}_{V,ij}$ is nonzero only if \mathbf{A}_{ij} is nonzero. Then we can obtain the sparse variable-to-constraint attention matrix $\mathbf{D}_V^{-1} \mathbf{M}_V$, where $\mathbf{D}_V \in \mathbb{R}^{n \times n}$ is the normalised diagonal matrix on the variable side with $\mathbf{D}_{V,ii} = \sum_{j=1}^m \mathbf{M}_{V,ij} + \epsilon$, and $\epsilon = 1e-8$ is a small positive constant to prevent zero denominator. Overall, the variable embedding update in the variable-to-constraint attention part is as follows:

$$\mathbf{H}_{\text{cross},t}^V = \mathbf{D}_V^{-1} \mathbf{M}_V \mathbf{V}_C. \quad (11)$$

Similarly, the constraint embedding update in the constraint-to-variable attention part is as follows:

$$\mathbf{H}_{\text{cross},t}^C = \mathbf{D}_C^{-1} \mathbf{M}_C \mathbf{V}_V. \quad (12)$$

By introducing the sparse matrix \mathbf{A} , the time complexity and memory complexity of our cross-attention part are reduced to $O(ed)$ and $O(e)$ respectively, where e denotes the number of nonzero elements in \mathbf{A} .

As with self-attention, we employ H attention heads to enhance representational capacity. These outputs are subsequently processed through residual connections and normalisation to yield the final embedded representations.

$$\mathbf{H}_{\text{cross},t}^V = \text{LayerNorm} \left(\mathbf{H}_{t-1}^V + \left(\parallel_{h=1}^H \mathbf{H}_{\text{cross},t,h}^V \right) \mathbf{W}_t^V \right), \quad (13)$$

$$\mathbf{H}_{\text{cross},t}^C = \text{LayerNorm} \left(\mathbf{H}_{t-1}^C + \left(\parallel_{h=1}^H \mathbf{H}_{\text{cross},t,h}^C \right) \mathbf{W}_t^C \right). \quad (14)$$

where \mathbf{W}_t^V and \mathbf{W}_t^C are trainable parameters used to map the Hd -dimensional feature back to d .

Parallel Inference and Feature Fusion. A key design in our dual-attention mechanism is the parallel inference scheme, where the self-attention and cross-attention modules work concurrently, as shown in Fig. 2a. Conventional BGNN-based scheme uses a two stage message passing scheme (variables \rightarrow constraints, constraints \rightarrow variables) to extract node embeddings. The constraint nodes practically work as intermediate messengers, forming information bottlenecks and incurring over-squashing issue. In contrast, our parallel design ensures that the intra-type and inter-type relationships are learned separately before fused together, effectively reducing interference between the two aspects and mitigating the information bottleneck issue.

As the final operation in our dual-attention mechanism, we fuse the learned embeddings as follows:

$$\mathbf{H}_t^V = \text{FFN}(\text{MLP}^V(\mathbf{H}_{\text{self},t}^V \parallel \mathbf{H}_{\text{cross},t}^V)), \quad (15)$$

$$\mathbf{H}_t^C = \text{FFN}(\text{MLP}^C(\mathbf{H}_{\text{self},t}^C \parallel \mathbf{H}_{\text{cross},t}^C)), \quad (16)$$

where FFN denotes Position-wise Feed-Forward Network.

Overall Complexity. Given an MILP instance with n variables, m constraints, and e nonzero coefficients in \mathbf{A} , the total time and memory complexities of our dual-attention layer are $O((m+n+e)d^2)$ and $O((m+n+e)d)$ respectively. Consequently, our proposed model exhibits favorable time and memory efficiency, enabling scalability to large MILP instances.

3.2 Application to Downstream Tasks

As a foundational backbone neural architecture, the variable embeddings \mathbf{H}_T^V and constraint embeddings \mathbf{H}_T^C obtained after the T dual-attention layers can be utilized in various ways to support downstream tasks. In this paper, we apply our model to the following types of representative learning tasks, as shown in Fig. 2b.

Instance-Level Prediction. These type of tasks focus on predicting a key property of an MILP instance, often in the form of supervised learning. For these tasks, we apply mean pooling to the n variable embeddings and m constraint embeddings respectively to obtain two vectors, which are then concatenated as the instance representation and fed into an MLP to obtain the final prediction:

$$\Phi_{\text{inst}} = \text{MLP}(\text{MEAN}(\mathbf{H}_T^V) \parallel \text{MEAN}(\mathbf{H}_T^C)) \quad (17)$$

where $\text{MEAN}(\mathbf{H}_T^V) = \frac{1}{n} \sum_{i=1}^n \mathbf{h}_{T,i}^V$, $\text{MEAN}(\mathbf{H}_T^C) = \frac{1}{m} \sum_{j=1}^m \mathbf{h}_{T,j}^C$. Here we consider two representative instance-level tasks following [41]: 1) instance feasibility prediction, which is a binary classification task and $\Phi_{\text{inst}} \in [0, 1]$ is the probability of being feasible; 2) optimal objective value prediction, which is a regression task and $\Phi_{\text{inst}} \in \mathbb{R}$ is the predicted objective value.

Element-Level Prediction. Another type of useful task is predicting element-level targets directly from the learned variable or constraint embeddings. The most commonly studied task in this direction is to predict the values of binary variables in the optimal solution \mathbf{x}^* via supervised learning:

$$\Phi_{\text{sol}} = \text{MLP}(\mathbf{H}_T^{BV}), \quad (18)$$

where $\mathbf{H}_T^{BV} = [\mathbf{h}_{T,i}^V | \text{if } \mathbf{x}_i \text{ is binary}]$ is the collection of binary variable embeddings, and $\Phi_{\text{sol}} \in [0, 1]^{n_b}$ is the probability vector of all the n_b binary variables. This task is attractive because binary variables are the great majority in practice [15, 16] and a precise prediction of binary variable values could significantly enhance solver's efficiency. A representative method is Prediction-and-Search (PaS) [19]. It fixes the k_0 lowest-probability variables to 0, k_1 highest-probability variables to 1, while allowing the solver to flip up to Δ of these fixed variables to mitigate the possible inaccurate

prediction by adding a linear constraint. Alternating Prediction Correction Neural Solving Framework (Apollo) [21] is a further improvement of PaS. It utilizes solver’s results within a short probing timeframe to correct the model’s predictions, thereby reducing inaccurate or unconfident predictions and enhancing the acceleration effects.

Solving State-Level Prediction. Branch-and-bound (B&B) algorithms are the core of modern MILP solvers. It is a complicated tree search process involving many decisions that can affect the solving efficiency. Deep learning can be of great value here by predicting high-quality decisions at each B&B solving state, which can naturally be formulated as a sequential decision-making problem. We apply our method to learning-to-branch [25], the most widely studied task of this type, which aims to predict the best variable for branching at each B&B node to minimize the search tree size. This can be achieved by associating solving state-dependent features to the variables and constraints, employing our neural architecture to extract corresponding embeddings, and then conducting the following computation:

$$\Phi_{\text{state}} = \text{softmax}(\text{MLP}(\mathbf{H}_{\text{state}, T}^V), \mathbf{P}_{\text{state}}) \quad (19)$$

where $\mathbf{H}_{\text{state}, T}^V$ is the state-dependent variable embeddings, and $\mathbf{P}_{\text{state}}$ is a n -dimensional binary vector to mask out variables that already have fixed values at that state, such that the resulting Φ_{state} represents a distribution over candidate variables. This policy network can be trained via imitation or reinforcement learning.

4 Results

This section reports extensive experiments on MILP instances from various backgrounds and sources to evaluate our attention-based model against BGNN, the de facto architecture for MILP. We consider the three types of tasks in Section 3.2, and use the same architecture with $T = 4$ dual-attention layers, $H = 2$ attention heads and $d = 64$ embedding dimension throughout the experiments. For BGNN, we follow the configuration adopted in all our baselines [19, 21, 25, 41] and use 2 layers with embedding dimension $d = 64$ same as ours. Other hyperparameters and implementation environments are provided in Appendix D. Raw features of variables and constraints for each task are listed in Appendix A. Our source code is publicly available at <https://github.com/hpx2024/Dual-Attention>.

4.1 Performance on Instance-Level Prediction

In this part, we follow the protocol in [41] to assess our method on feasibility prediction and optimal objective value prediction, two representative instance-level prediction tasks. Chen et al. [41] find that the so-called foldable MILPs are hard for vanilla BGNN due to undistinguishable symmetry, and propose to append a random feature to the raw feature of each variable and constraint to enhance the power of BGNN. We also add this random feature to our model for fair comparison. We follow the procedure in [41] (presented in Appendix B.1) to generate synthetic MILP instances with $n = 20$ variables and $m = 6$ constraints separated into two datasets \mathcal{D}_1 (unfoldable) and \mathcal{D}_2 (foldable). Both sets have 2000 instances, among which we use 1000 instances for

Table 1: Performance of Feasibility and optimal objective value prediction

| Dataset | Method | Feasibility prediction | | Optimal objective prediction | |
|------------------------------|-----------|-------------------------|--|------------------------------|------------------|
| | | Error-Rate \downarrow | | | MSE \downarrow |
| \mathcal{D}_1 (Unfoldable) | BGNN [41] | 0.0% | | 3.975e-09 | |
| | Ours | 0.0% | | 3.889e-14 | |
| \mathcal{D}_2 (Foldable) | BGNN [41] | 6.0% | | 1.178e-11 | |
| | Ours | 0.0% | | 2.312e-13 | |

training and the remaining for testing. To collect supervised training labels, we use the SCIP solver [46] to determine the feasibility and obtain optimal solutions for each feasible instance.

Results summarized in Table 1 show that for feasibility prediction, both models can achieve perfect accuracy on the simpler dataset \mathcal{D}_1 . However, On the more challenging dataset \mathcal{D}_2 , our model can still correctly predict the feasibility of all testing instances, whereas the model in [41] incurs a 6% error rate. For optimal objective value prediction, the Mean Square Error (MSE) of our method is five and two orders of magnitude smaller than that of the enhanced BGNN in [41] on \mathcal{D}_1 and \mathcal{D}_2 , respectively. These results demonstrate the superior accuracy and robustness of our model in instance-level prediction tasks.

4.2 Performance on Element-Level Prediction

In this part, we consider the well-studied task of binary variable prediction, following the setting in state-of-the-art works PaS [19] and Apollo [21]. We conducted experiments on four representative and commonly used datasets: balanced Item Placement (IP), Workload Appointment (WA), Maximum Independent Set (MIS), and Combinatorial Auction (CA). The first two datasets originate from the NeurIPS ML4CO 2021 competition [47], while the latter two were generated using the Ecole library [48] following the protocol in [25]. These problems possess profound practical significance. As outlined in [47], IP simulates resource allocation challenges within Google’s large-scale cloud computing systems, whilst WA models the apportionment of data flows between servers. MIS is a classic problem in graph theory, applicable to many cases such as communication network design and social network analysis. CA corresponds to economic system design, with practical applications such as electronic auctions and spectrum allocation. These problems underpin core industrial demands, demonstrating the broad practical value of combinatorial optimization. For all the four problems, we use 400 instances for training and 100 for testing. Detailed introduction of these problems and the data generation protocol can be found in Appendix B.2. We use Gurobi (v12.0.1) [49], the state-of-the-art commercial MILP solver, with 3,600 seconds time limit to collect supervised training labels and as the backbone solver in the following predict-and-search experiments. We train BGNN and our model under the PaS framework [19], the former is also the prediction model utilized in Apollo [21].

Table 2: Performance evaluation on binary variable prediction

| Dataset | Method | MCC \uparrow | Bal-Acc \uparrow | Macro-F1 \uparrow | MSE \downarrow | Error-Num \downarrow | Error-Rate \downarrow |
|---------|-----------|----------------|--------------------|---------------------|------------------|------------------------|-------------------------|
| IP | BGNN [19] | 0.0156 | 0.5058 | 0.5060 | 0.0900 | 21927 | 20.88% |
| | Ours | 0.0178 | 0.5089 | 0.5089 | 0.0900 | 18610 | 17.72% |
| WA | BGNN [19] | 0.7972 | 0.8978 | 0.8986 | 0.0492 | 6089 | 6.83% |
| | Ours | 0.8411 | 0.9164 | 0.9205 | 0.0386 | 4737 | 5.32% |
| MIS | BGNN [19] | 0.6431 | 0.8216 | 0.8215 | 0.1234 | 53150 | 17.72% |
| | Ours | 0.6920 | 0.8461 | 0.8460 | 0.1058 | 45868 | 15.29% |
| CA | BGNN [19] | 0.3488 | 0.6778 | 0.6742 | 0.1429 | 59828 | 23.10% |
| | Ours | 0.3825 | 0.6946 | 0.6911 | 0.1383 | 56624 | 21.86% |

Table 3: Average PG and PI (for each problem, the value within parenthesis is the BKV)

| Method | IP (12.24) | | WA (700.96) | | MIS (1371.74) | | CA (220061.61) | |
|------------------|-----------------|-----------------|-----------------|-----------------|-----------------|-----------------|-----------------|-----------------|
| | PG \downarrow | PI \downarrow |
| Gurobi (3600s) | 6.944% | 144.45 | 0.026% | 2.74 | 0% | 0.46 | 0.222% | 4.34 |
| PaS-BGNN [19] | 7.435% | 146.27 | 0.021% | 2.64 | 0% | 0.02 | 0.246% | 4.73 |
| PaS-Ours | 5.556% | 106.13 | 0.016% | 2.60 | 0% | 0.01 | 0.232% | 4.29 |
| Apollo-BGNN [21] | 4.984% | 112.36 | 0.020% | 2.75 | 0.008% | 0.53 | 0.316% | 5.21 |
| Apollo-Ours | 4.167% | 102.87 | 0.019% | 2.73 | 0% | 0.44 | 0.249% | 4.53 |

We first evaluate the accuracy of our method in predicting the optimal values of binary variables. This is a binary classification task with two notable characteristics. First, the 0/1 labels are not inherently positive or negative, as both classes are of equal importance and the goal is simply to predict correct variable values as much as possible. Second, class labels can be imbalanced. For IP, WA, MIS and CA, the ratios of 1 to 0 variables are 9:1, 1:4, 3:1 and 1:1, respectively. To provide a comprehensive assessment, we use balanced accuracy (Bal-Acc), macro F1-score (Macro-F1), and Matthews correlation coefficient (MCC) as evaluation metrics. We also report the MSE between the predicted probability vector Φ_{sol} and the target optimal solution \mathbf{x}^* , as well as the number and rate of incorrectly predicted variables (Error-Num and Error-Rate). As shown in Table 2, our attention-based model consistently outperforms BGNN across all datasets and all metrics. As a more intuitive observation, our model predicts 15.1%, 22.2%, 13.7% and 5.4% more variables correctly than BGNN on IP, WA, MIS and CA respectively, demonstrating a much stronger prediction accuracy.

Next, we evaluate the impact of solution prediction on downstream MILP solving performance. The trained BGNN and our attention-based model are integrated into the PaS [19] and Apollo [21] frameworks to solve the 100 testing instances using Gurobi with a time limit of 1000 seconds. The original Gurobi with 3600 seconds time limit is also included as a non-learning baseline. All hyperparameters are fine-tuned on each dataset, as detailed in Appendix D.2. For each method, we report the geometric mean of the Primal Gap (PG) and the Primal Integral (PI) [50] as

Table 4: Improvement over BGNN based Predict-and-Search methods

| Dataset | PG Improvement | | PI Improvement | |
|---------|----------------|------------------|----------------|------------------|
| | PaS-BGNN [19] | Apollo-BGNN [21] | PaS-BGNN [19] | Apollo-BGNN [21] |
| IP | 25.275% | 16.393% | 27.442% | 8.446% |
| WA | 26.667% | 7.143% | 1.515% | 0.727% |
| MIS | 0% | 100% | 50% | 16.981% |
| CA | 5.907% | 21.035% | 9.302% | 13.052% |
| Average | 14.462% | 36.143% | 22.065% | 9.802% |

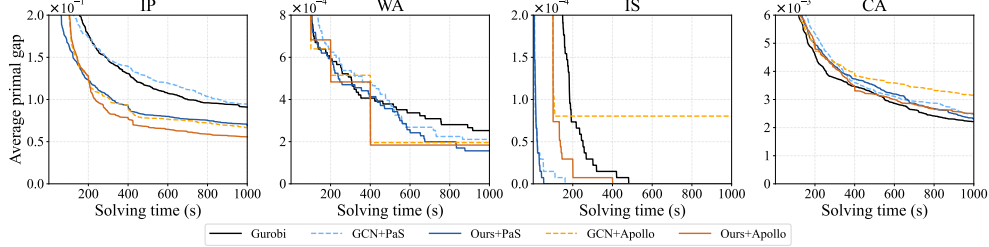


Fig. 3: Average Primal Gap (PG) of each method as a function of solving time. Each panel visualizes the solving process of a dataset. The black solid line is Gurobi, while other solid and dashed lines correspond to our attention-driven architecture and the BGNN baseline, respectively, combined with two predict-and-search frameworks (PaS and Apollo). Using our model achieves consistently smaller PG and faster convergence across all problems, indicating improved optimization efficiency and better integration with Gurobi.

evaluation metrics. PG measures the final solution quality relative to the best-known value (BKV), which is set as the best result returned by all methods. PI quantifies the solver’s efficiency in converging toward the optimum over time. Further details of these metrics are provided in Appendix C. Results of this part are shown in Table 3, and the solving process of each method is visualized in Fig. 3. Clearly, our attention-based architecture consistently outperforms the two BGNN based counterparts across all problems. The substantial PG and PI improvements (Table 4) indicate that the accurate prediction of our model not only leads to better solutions, but also accelerates the solver’s convergence. In particular, with our neural architecture, both PaS and Apollo surpass Gurobi on three problems (IP, WA, and MIS), whereas their BGNN-based versions outperform Gurobi on only two.

4.3 Performance on Solving State-Level Prediction

In this part, we evaluate our model on learning-to-branch, a representative solving state-level prediction task. We apply our attention-driven model to the Imitation Learning (IL) framework in [25], and compare the performance with its original BGNN.

Table 5: Imitation learning accuracy on the test sets (higher is better)

| Method | SC | | | CA | | | CFL | | | MIS | | |
|-----------|--------------|--------------|--------------|--------------|--------------|--------------|--------------|--------------|--------------|--------------|--------------|--------------|
| | acc@1 | acc@5 | acc@10 |
| BGNN [25] | 70.35 | 93.16 | 98.39 | 70.07 | 93.11 | 98.49 | 53.50 | 88.70 | 96.40 | 81.00 | 92.40 | 95.70 |
| Ours | 71.51 | 93.75 | 98.61 | 70.20 | 93.90 | 98.60 | 57.20 | 90.30 | 96.90 | 82.70 | 93.20 | 96.10 |

Table 6: Comparison of B&B tree size (i.e., number of nodes, lower is better)

| Method | Test | | | |
|-----------|-----------------|------------------|------------------|-------------------|
| | SC | CA | CFL | MIS |
| BGNN [25] | 65.4±11% | 57.8±16% | 350.4±43% | 48.6±47% |
| Ours | 64.9±10% | 57.3±13% | 323.1±39% | 48.4±45% |
| Method | Transfer | | | |
| | SC | CA | CFL | MIS |
| BGNN [25] | 160.9±10% | 836.5±14% | 545.7±48% | 10280.5±73% |
| Ours | 152.3±7% | 811.7±12% | 512.5±48% | 8938.5±42% |

It learns a fast neural approximation of the Strong Branching (SB) strategy, which produces compact search trees but is computationally expensive. While there are a number of subsequent works in learning-to-branch, they mostly focus on training mechanisms and the underlying neural architecture largely remains the BGNN proposed in [25]. To fairly assess the representation learning capability of different neural architectures, we therefore conduct experiments within this well-established framework.

Following [25], we conduct experiments on four NP-hard problems: Set Covering (SC), Combinatorial Auctions (CA), Capacitated Facility Location (CFL), and Maximum Independent Set (MIS). SC and CFL, as described previously for CA and MIS, also hold significant practical importance in real-world applications. SC is widely used for service coverage optimization, such as emergency response, healthcare, and communication network planning. CFL is fundamental to supply chain and logistics network design, where capacity-constrained facilities must efficiently satisfy spatially distributed demands. Detailed formulation and instance generation procedure are listed in Appendix B. Our experiments follow the protocol in [25]. For each problem, we generate 10000 instances for training and 40 for testing. Additionally, we generated 40 instances larger and more challenging than the training set instances to form the transfer set. Since learning-to-branch requires direct access to the solver’s internal logic, we use the state-of-the-art open-source solver SCIP [46] as the environment, and collect SB demonstrations using its built-in implementation.

We compare with BGNN in the learning-to-branch task from two aspects as in [25]. First, in terms of prediction accuracy, Table 5 reports the acc@1, acc@5, and acc@10 metrics, representing the proportion of times that the correct SB label appears in the

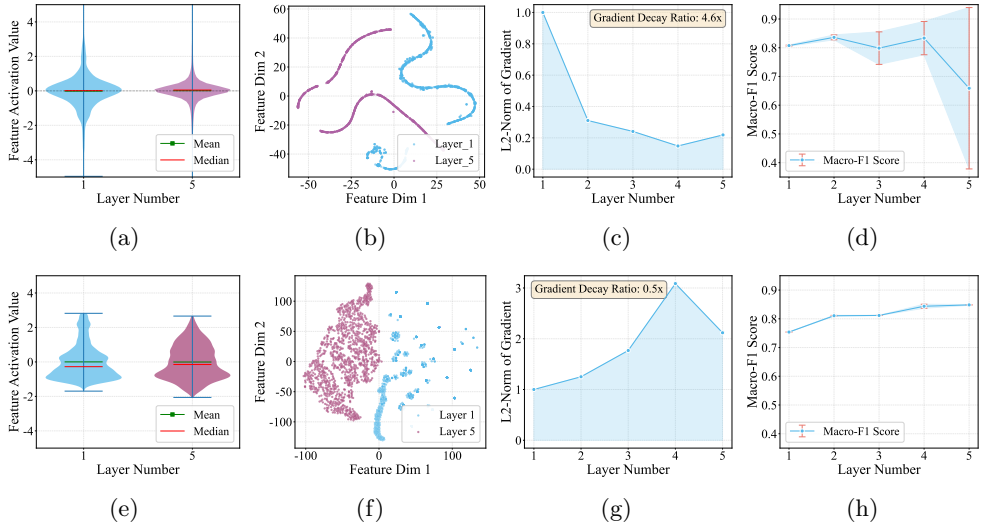


Fig. 4: Comparison of the performance in extracting deep representations. (a) and (e) depict the normalized embedding values of the BGNN and our model at the 1st and 5th layer. (b) and (f) depict the t-SNE visualization of embeddings at the 1st and 5th layer of BGNN and our model. (c) and (g) depict the decay of gradients in the BGNN and our model as the network deepens. (d) and (h) depict the mean Macro-F1 score with standard deviation of training BGNN and our model five times under different numbers of layers.

top-1, top-5, and top-10 ranked predictions. Under the same training framework, our model consistently achieves higher accuracy across all problems. Second, the learned policy is embedded in SCIP to solve the test and transfer instances. As shown in Table 6, the B&B search trees under the guidance of our method are consistently smaller than those of BGNN, with the advantage becoming more pronounced on the larger transfer instances.

4.4 Mechanism Analysis

To understand why our attention-driven architecture effectively outperforms BGNN, we perform fine-grained analysis on the binary variable prediction task, to evaluate the capabilities of the two architectures in extracting deep representations and capturing long-range dependencies, as well as ablation studies of our attention-based architecture.

4.4.1 Extracting Deep Representations

We visualize the performance of BGNN and our model on the MIS problem under different numbers of layers (from 1 to 5) in Fig. 4. First, Fig. 4a and 4e show the violin plot of Z-score normalized embedding values obtained at the 1st and 5th layer. For BGNN, embedding values at the 5th layer are more concentrated than the 1st layer,

indicating a trend of collapsing into similar representations. In contrast, our model exhibits minimal variation in embedding value distributions across shallow and deep layers, indicating a much stronger ability in preserving feature diversity and mitigating the over-smoothing issue.

Second, Fig. 4b and 4f show the t-SNE visualization of the embeddings obtained at the 1th and 5th layer projected to the same 2D space. For BGNN, embeddings tend to collapse into one-dimensional manifolds, with a clear decrease in the spatial coverage from shallow to deep layers. This indicates a decline of diversity in the feature space and further validating the phenomenon of over-smoothing. In contrast, our model exhibits a much more diverse distribution in the feature space, effectively mitigating the feature collapse issue of BGNN.

Third, Fig. 4c and 4g report the gradient flow analysis by plotting the L2-norm of gradient at each layer, normalized by the value of the first layer. A clear distinction between the two models can be observed. BGNN’s gradient rapidly and almost monotonically decays from layer 1 to 5, which severely affects backpropagation through deeper layers and largely explains why it struggles to utilize more than 2 layers. In contrast, the gradient strength in our model stably increases and peaks at the 4th layer before a moderate decline at the 5th layer, showing that our design enables effective backpropagation through more layers, enabling the network to learn deeper and richer representations.

Finally, we evaluate the prediction performance of each method under different depths. Specifically, for each layer number, we train each model 5 times, and plot the average Macro-F1 score with standard deviation in Fig. 4d and 4f. Evidently, BGNN is highly unstable beyond two layers with a marked decline at the 5th layer. Therefore, aligning with most existing works (e.g., [19, 21, 25, 41]), we use BGNN with two layers in our experiments. In contrast, our model performs highly consistent and robust with small deviation, and the prediction quality stably increases with the number of layers. Although stacking more layers could further enhance performance, we uniformly use a four-layer model for our method for a reasonable balance between representation learning power and model complexity.

4.4.2 Capturing Long-Range Dependencies

We perform gradient-based attribution [51], a method for deep model explanation, to analyze the capability of the two-layer BGNN and our four-layer attention architecture in capturing long-range dependencies. Specifically, we randomly draw an instance from the WA test set, and the longest distance between two nodes in the underlying bipartite graph is 7 hops. On this instance, we backpropagate the prediction results for each variable x_i through the trained model, calculating the L2 norm of the feature gradients of other variables or constraints to measure their influence on x_i . Fig. 5a and 5b illustrate the average influence of variables (i.e., nodes that are 2, 4, 6 hops away) of BGNN and our method, whilst Fig. 5c and 5d demonstrate the average influence of constraints (nodes that are 1, 3, 5, 7 hops away) of the respective models. It is evident that for BGNN, the influence of nodes decays sharply with distance, and the variables or constraints beyond 3 hops exert negligible impact on BGNN’s prediction since the influence almost vanishes. Though a two-layer BGNN theoretically propagates

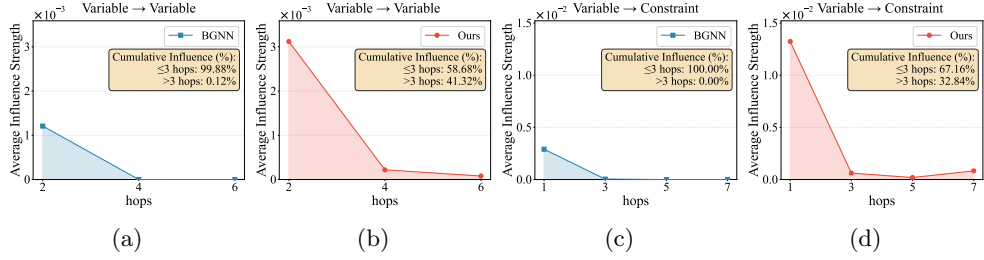


Fig. 5: Analysis of long-range dependency modeling in BGNN and our attention-based architecture. Gradient-based attribution is used to quantify the influence strength between a target variable and other nodes at different distances. Panels (a) and (b) show average variable-to-variable influence for BGNN and our model, while panels (c) and (d) show average variable-to-constraint influence. BGNN exhibits rapidly diminishing influence with increasing distance, while the attention-based model maintains non-negligible influence across farther hops. Insets report the cumulative influence contributed by nodes within and beyond three hops.

information across up to 4 hops, in practice the signal from 4-hop nodes is almost completely suppressed. In contrast, our attention architecture maintains substantial non-zero influence even at the farthest 7 hops, demonstrating its ability to effectively capture long-range dependencies that BGNN fails to exploit.

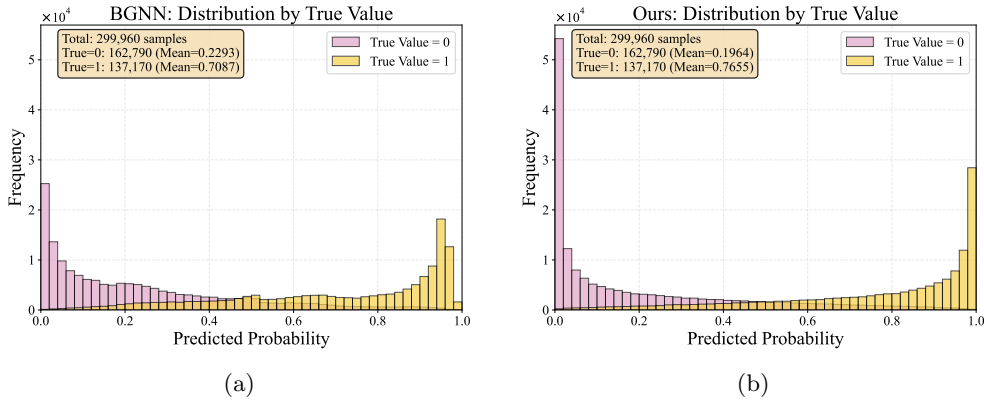


Fig. 6: Distribution of predicted probabilities for binary variables. Histograms show the predicted probability of each binary variable being 1, separated by true labels, for BGNN (a) and our attention-based architecture (b). BGNN exhibits more overlap between the two distributions, with many samples lying in the ambiguous 0.3–0.7 region. In contrast, our model produces sharply separated and highly concentrated distributions near 0 and 1, indicating a stronger discriminative power.

4.4.3 Predicted Probability Analysis

Fig. 6 compares the distribution of predicted probabilities for BGNN and our attention-driven architecture on the MIS problem. For BGNN, the predicted probabilities for true-0 and true-1 variables exhibit substantial overlap, with many samples falling in the ambiguous 0.3–0.7 range, indicating low confidence and limited discriminative ability. In contrast, our model produces highly concentrated and well-separated distributions: true-0 variables are sharply peaked near 0, and true-1 variables near 1, with significantly smaller overlap in the middle range. This demonstrates that the attention-based architecture yields more calibrated and confident predictions, and is significantly more effective at capturing the structural patterns that determine binary variable values in MILPs.

4.4.4 Ablation Studies

First, we perform architectural ablation experiments on the WA dataset by independently removing the self-attention and cross-attention modules from our architecture. Table 7 shows that removing either component leads to significant performance drop, demonstrating that both modules contribute critically and that their joint use is essential for achieving the full effectiveness of our model.

Table 7: Ablation results on binary variable prediction using the WA Dataset

| Method | MCC \uparrow | Bal-Acc \uparrow | Macro-F1 \uparrow | MSE \downarrow | Error-Num \downarrow | Error-Rate \downarrow |
|----------------|----------------|--------------------|---------------------|------------------|------------------------|-------------------------|
| Ours | 0.8411 | 0.9164 | 0.9205 | 0.0386 | 4737 | 5.32% |
| Ours w/o self | 0.7985 | 0.8964 | 0.8992 | 0.0486 | 6023 | 6.76% |
| Ours w/o cross | 0.5724 | 0.7806 | 0.7860 | 0.0984 | 12629 | 14.18% |

Next, we perform alternative design ablation on WA to evaluate other ways of alleviating the limitation of BGNN. First, we employ Graph Attention Network (GATv2) [52] to enhance the learning power of BGNN by allowing each node to weight its neighbors through attention (named BGAT). Second, we augment BGNN by adding an intra-element self-attention module to each of its two message passing steps in Eq. (2) (named BGNN+self), to allow each variable and constraint to globally interact with other elements of the same type. Finally, motivated by the recent success of Graph Transformer (GT) in mitigating over-smoothing and over-squashing issues of GNN, we modify Polynormer [45], a high-performing GT, into a bipartite architecture (named BGT) that mimics the variable-to-constraint and constraint-to-variable embedding process of BGNN. BGAT provides more flexible message aggregation, while BGNN+self and BGT provide global receptive fields. However, results in Table 7 show that none of them yields a noticeable improvement in representation quality. This is because they still follow the graph-based bipartite update scheme and rely on sequential message aggregation. In contrast, our method moves away from the graph view, and enables direct global interactions among elements within and across types

Table 8: Performance of binary variable prediction on the WA Dataset

| Method | MCC \uparrow | Bal-Acc \uparrow | Macro-F1 \uparrow | MSE \downarrow | Error-Num \downarrow | Error-Rate \downarrow |
|-----------|----------------|--------------------|---------------------|------------------|------------------------|-------------------------|
| BGNN | 0.7972 | 0.8978 | 0.8986 | 0.0492 | 6089 | 6.83% |
| BGAT | 0.7947 | 0.8947 | 0.8973 | 0.0492 | 6138 | 6.89% |
| BGNN+self | 0.8035 | 0.8997 | 0.9017 | 0.0488 | 5884 | 6.60% |
| BGT | 0.7408 | 0.8702 | 0.8704 | 0.0649 | 7797 | 8.75% |
| Ours | 0.8411 | 0.9164 | 0.9205 | 0.0386 | 4737 | 5.32% |

Table 9: Performance of binary variable prediction on the MIPLIB benchmark

| Method | MCC \uparrow | Bal-Acc \uparrow | Macro-F1 \uparrow | MSE \downarrow | Error-Num \downarrow | Error-Rate \downarrow |
|----------|----------------|--------------------|---------------------|------------------|------------------------|-------------------------|
| BGNN-MIS | 0.0846 | 0.5394 | 0.5276 | 0.1997 | 483164 | 12.27% |
| Ours-MIS | 0.1490 | 0.5641 | 0.5730 | 0.0760 | 289478 | 7.35% |
| BGNN-CA | 0.0001 | 0.5000 | 0.4987 | 0.1615 | 316100 | 8.03% |
| Ours-CA | 0.1508 | 0.5902 | 0.5728 | 0.1293 | 405113 | 10.29% |
| BGNN-WA | 0.0099 | 0.5061 | 0.5031 | 0.2412 | 486931 | 12.36% |
| Ours-WA | 0.1053 | 0.5549 | 0.5526 | 0.5174 | 363226 | 9.22% |

simultaneously, thereby effectively overcoming the representation learning bottleneck of graph-based models.

4.5 Real-world Instances

To further demonstrate the practicality of our attention-based model, we conducted binary variable prediction experiments on MIPLIB [53], a well-recognized benchmark with 240 challenging instances from various real-world scenarios. Binary variables are majority in MIPLIB: 164 out of the 240 instances are pure binary, and in 44 out of the remaining 76 instances, more than 90% of the integer variables are binary [16]. This underscores the practical relevance of accurately predicting binary variables in MILP. We use 215 MIPLIB instances for evaluation, with 25 instances left out due to no binary variable, no feasible solution with 3,600s Gurobi solving, or out-of-memory on our machine (listed in Appendix E). Given the substantial heterogeneity of MIPLIB instances, directly training prediction models is difficult. We therefore evaluate the out-of-distribution generalization ability of models pre-trained on the MIS, CA, and WA datasets. Models trained on IP are excluded because the positional encoding used to break symmetries in IP is not generally applicable to MIPLIB instances. It is worth noting that the ratio of 0 to 1 labels in the MIPLIB benchmark is approximately 42:1, which is extremely imbalanced. Results in Table 9 demonstrate that our attention-based model significantly outperforms BGNN, regardless of the pre-training sources. The lower error of BGNN-CA over Ours-CA is misleading: under the extreme class imbalance, predicting all variables as 0 yields superficially low error rates but provides no meaningful discriminative ability, as reflected by its near-zero MCC (0.0001), low balanced accuracy (0.5000), and low macro-F1 score (0.4987). In contrast, our CA model maintains significantly better predictive power despite the dataset shift and

label imbalance. Overall, these results demonstrate that our attention-based architecture generalizes robustly to MIPLIB instances that differ significantly from the training distributions, highlighting its potential for practical deployment in real-world MILP solving.

5 Discussion and Conclusion

In this study, we present an attention-driven representation learning method for MILP, a general combinatorial optimization model with numerous practical applications across science and engineering. At the core is an element-centric view, which leads to a dual-channel attention mechanism that simultaneously performs inter-type and intra-type attention for the variable and constraint elements, effectively addressing the limitations of GNN-based approaches in capturing global structural patterns and long-range dependencies. Comprehensive experiments on three types of representative tasks across various synthetic and real-world benchmarks demonstrate that the proposed model consistently yields superior predictions, and generalizes robustly to out-of-distribution problems.

The effectiveness of our approach stems from several key architectural mechanisms. The variable and constraint self-attention modules eliminate the locality imposed by graph message passing, allowing nodes to aggregate information globally from same-type elements in a single layer. Meanwhile, the symmetric cross-attention module explicitly encodes variable-constraint interactions from both directions, providing a richer representational signal than the one-directional neighborhood-based aggregation in GNN. The above modules work in parallel in our design, which jointly overcome the representation learning bottlenecks of GNNs, yielding more expressive embeddings and more precise predictions for different downstream tasks.

While demonstrating strong performance, our method can be further improved in several aspects. First, attention-based architectures incur greater computational cost than shallow GNNs, suggesting that improving efficiency via techniques such as sparsification is an important direction for future development. Second, while the model generalizes well to diverse MIPLIB instances, further investigation is required to understand its behavior on extremely large-scale and label-imbalanced industrial problems. Finally, exploiting additional theoretical and structural properties of MILP such as duality could further enhance the representation learning power.

Looking forward, as a general backbone model, our method can potentially be integrated more tightly into the branch-and-bound pipeline, enabling learning-based components such as algorithm configuration, cutting plane selection, and local improvement heuristics to further accelerate MILP solving in practice. Extending the framework to nonlinear or stochastic mixed-integer optimization represents another promising avenue. More broadly, considering that the variable-constraint-relation abstraction is pervasive in general combinatorial optimization, our results highlight the potential of attention-based mechanisms as a foundation for other general COPs such as Boolean/Maximum Satisfiability, Constraint Programming, and Answer Set Programming, opening opportunities for designing powerful learning-assisted algorithms beyond graph-based paradigms.

Appendix A Raw Features

The raw features of variables and constraints used in this paper align closely with the baseline representation in each predictive task. Specifically, the raw features used for instance-level, element-level and solving state-level prediction tasks follow Chen et al. [41], Han et al. [19], and Gasse et al. [25], as listed in Table A1, A2 and A3, respectively.

Table A1: Raw features for instance-level prediction

| ID | Variable Feature Name | Description |
|----|-----------------------|---|
| 0 | Objective | Objective function coefficient |
| 1 | Variable type | Indicates whether the variable is a binary variable |
| 2 | Lower bound | Lower bound of variable |
| 3 | Upper bound | Upper bound of variable |

| ID | Constraint Feature Name | Description |
|----|-------------------------|--|
| 0 | Right-hand constant | Constraint on the right-hand side constant |
| 1 | Constraint type | The sense of the constraint |

Table A2: Raw features for element-level prediction

| ID | Variable Feature Name | Description |
|------|---------------------------------|--|
| 0 | Objective function coefficients | Indicates the weight of this variable in the objective function |
| 1 | Variable coefficient | The mean coefficient of the variable across all constraints |
| 2 | Variable degree | Degree of a variable node in the bipartite graph |
| 3 | Maximum variable coefficient | The maximum coefficient value of the variable across all constraints |
| 4 | Minimum variable coefficient | The minimum coefficient value of the variable across all constraints |
| 5 | Variable type | Indicates whether the variable is a binary variable |
| 6-17 | Position embedding | Encoding binary variable order (only effective on IP) |

| ID | Constraint Feature Name | Description |
|----|-------------------------|---|
| 0 | Constraint coefficient | The mean value of the constraint coefficients |
| 1 | Constraint degree | The number of variables involved in the constraints |
| 2 | Right-hand constant | Constraint on the right-hand side constant |
| 3 | Constraint type | The sense of the constraint |

Table A3: Raw features for solving state-level prediction

| ID | Variable Feature Name | Description |
|-------|--------------------------------|--|
| 0-3 | Variable type | Employing one-hot encoding to denote whether a variable type is binary, integer, impl.integer, or continuous |
| 4 | Objective coefficient | Normalised objective function coefficients |
| 5 | Lower bound | Indicates whether there is a lower bound |
| 6 | Upper bound | Indicates whether there is an upper bound |
| 7 | At the lower bound | Indicates whether the current solution value equals the lower bound |
| 8 | At the upper bound | Indicates whether the current solution value equals the upper bound |
| 9 | Solution value fractionality | Indicates the extent of deviation from an integer |
| 10-13 | Basis status | Representing the basis states of the simplex method (lower, basic, upper, zero) using one-hot encoding. |
| 14 | Reduced cost | Marginal cost of non-basic variables. |
| 15 | Age | Indicates how many times the variable (or node) has undergone LP solving |
| 16 | Relaxation value | The solution value obtained after solving the LP relaxation problem for the variable at the current node |
| 17 | Optimal integer solution value | The values assumed by variables in the currently found optimal integer feasible solution |
| 18 | Average integer solution value | Average of historical integer solutions |
| ID | Constraint Feature Name | Description |
| 0 | Cosine similarity | Cosine similarity with respect to the objective function |
| 1 | Right-hand constant | Normalised constraint right-hand side constant |
| 2 | Tight | Indicates whether the constraint is tight |
| 3 | Dual solution value | Normalised dual solution value |

Appendix B Description of Benchmark Problems

B.1 Instance-Level Prediction

For instance-level prediction tasks, we follow the data generation protocol in Chen et al. [41] to generate instances with $n = 20$ variables and $m = 6$ constraints. Specifically, the procedure of generating unfoldable instances is as follows:

- The objective function coefficient c_i of each variable x_i is sampled from a normal distribution $\mathcal{N}(0, 0.01)$;
- The lower bound l_i and upper bound u_i of each variable x_i are independently sampled from a normal distribution $\mathcal{N}(0, 10)$. If l_i is sampled greater than u_i , then l_i and u_i are swapped to ensure $l_i \leq u_i$;
- Each variable x_i has a 50% probability of being assigned as an integer variable; otherwise, it is a continuous variable;
- The right-hand side constant term b_j of each constraint is sampled from a standard normal distribution $\mathcal{N}(0, 1)$;
- The constraint type is uniformly selected from the set $\{\leq, =, \geq\}$;

- The adjacency matrix \mathbf{A} is initialized as a 6×20 zero matrix, with 60 positions randomly selected as nonzero elements. Each nonzero element \mathbf{A}_{ij} is sampled from a standard normal distribution $\mathcal{N}(0, 1)$.

The foldable instances are generated in pairs. Specifically, we generate k pairs of instances where $1 \leq k \leq 500$, and the procedure of generating each foldable instance is as follows:

- The objective function coefficient c_i of each variable x_i is set to 0;
- A subset $J = \{x_{j1}, x_{j2}, \dots, x_{j6}\}$ of 6 variables is randomly selected from the 20 variables;
- Each $x_{ji} \in J$ is set to be a binary variable;
- Each $x_{ji} \notin J$ is set to be a continuous variable, with l_i and u_i generated the same as unfoldable instances;
- The $(2k - 1)$ -th instance is feasible, and its constraints form a hexagonal loop: $x_{j1} + x_{j2} = 1, x_{j2} + x_{j3} = 1, x_{j3} + x_{j4} = 1, x_{j4} + x_{j5} = 1, x_{j5} + x_{j6} = 1, x_{j6} + x_{j1} = 1$;
- The $2k$ -th instances is infeasible, and its constraints form two triangular cycles: $x_{j1} + x_{j2} = 1, x_{j2} + x_{j3} = 1, x_{j3} + x_{j1} = 1, x_{j4} + x_{j5} = 1, x_{j5} + x_{j6} = 1, x_{j6} + x_{j4} = 1$.

B.2 Element-Level Prediction

In node-level prediction tasks, we will provide problem descriptions for the Maximum Independent Set (MIS), Combinatorial Auction (CA), Balanced Item Placement (IP), and Workload Appointment problems (WA). For the former two, instances are generated using the Ecole library following the methodology of Gasse et al. [25]. Instances for the latter two can be directly downloaded from the ML4CO competition website [47]. For all instances, we utilise 400 for training and 100 for testing. Additionally, both the IP and WA datasets were trained using instances labelled 0 to 399, with testing conducted on 100 instances from the valid folder. Below we outline the generative models for each problem and the specific generative parameters for the IS and CA problems.

B.2.1 Maximum Independent Set

In the MIS problem, given an undirected graph $G \equiv (V, E)$, the objective is to select a maximal subset $V' \subset V$ such that no two nodes in the subset are adjacent, i.e., no edge connects them. The generative model for MIS problems [54] is formulated as the following mixed-integer linear programming problem:

$$\begin{aligned} \max_x \quad & \sum_{v \in V} x_v \\ \text{s.t.} \quad & x_u + x_v \leq 1 \quad \forall (u, v) \in E \\ & x_v \in \{0, 1\} \quad \forall v \in V \end{aligned}$$

The binary variable x_v indicates whether node v is selected into the independent set (1 denotes selected, 0 denotes not selected). The constraints ensure that for each edge (u, v) , nodes u and v cannot be selected simultaneously. We generated instances that are as challenging as possible for our hardware. The specific parameters for the

MIS problem are number of nodes $n = 3000$, and the probability of an edge existing between any two nodes in the graph is set to 0.1.

B.2.2 Combinatorial Auction

In the CA problem, given m items, there are n bids $\{(B_i, p_i) : i \in [n]\}$, where B_i denotes a subset of items and p_i is the price for that combination. The objective is to assign items to bids to maximize revenue, with each item being assigned at most once. The MILP model for CA [55] is formulated as:

$$\begin{aligned} \max_x \quad & \sum_{i=1}^n p_i x_i \\ \text{s.t.} \quad & \sum_{i:j \in B_i} x_i \leq 1 \quad \forall j \in [m] \\ & x_i \in \{0, 1\} \quad \forall i \in [n] \end{aligned}$$

The binary variable x_i indicates whether bid i is accepted (1 for acceptance and 0 otherwise). The constraints ensure that each item j is included in at most one accepted bid. The specific parameters generated for the CA problem are: $m = 8000, n = 3000$, with the price value randomly chosen from $\text{min_value} = 1$ and $\text{max_value} = 100$.

B.2.3 Balanced Item Placement

The IP problem simulates the placement of items (such as data files or computational processes) within containers (such as hard disks or servers) in a large-scale distributed system, such as a data centre. The objective is to achieve the most balanced utilization of containers, whilst satisfying various capacity constraints, thereby avoiding hotspots or resource waste. The problem also incorporates a practical constraint: the system currently possesses an existing placement scheme, but permits re-optimization of this placement within a finite relocation cost (i.e., a limit on the maximum number of items that may be moved). An IP instance comprises three sets: the item set I , the container set J , and the dimension set K (e.g., CPU, memory, disk I/O, etc.). Then the MILP formulation of IP is:

$$\begin{aligned} \min_{x,y,z} \quad & \sum_{j \in J} \sum_{k \in K} \alpha_k y_{jk} + \sum_{k \in K} \beta_k z_k \\ \text{s.t.} \quad & \sum_{j \in J} x_{ij} = 1 \quad \forall i \in I \\ & \sum_{i \in I} a_{ik} x_{ij} \leq b_k \quad \forall j \in J, \forall k \in K \\ & \sum_{i \in I} d_{ik} x_{ij} + y_{jk} \geq 1 \quad \forall j \in J, \forall k \in K \\ & y_{jk} \leq z_k \quad \forall j \in J, \forall k \in K \\ & x_{ij} \in \{0, 1\} \quad \forall i \in I, \forall j \in J \\ & y_{jk} \geq 0 \quad \forall j \in J, \forall k \in K \end{aligned}$$

The binary variable x_{ij} indicates whether item i is placed in container j (1 for true and 0 for false). The parameter a_{ik} denotes the size or demand of item i along dimension k , while b_k represents the capacity limit for each container in dimension k . The

parameter d_{ik} is the imbalance contribution coefficient of item i on dimension k . The continuous, non-negative variable y_{jk} measures the extent to which the total imbalance contribution of items in container j for dimension k falls below a predefined threshold (value of 1 in the constraint $\sum_i d_{ik}x_{ij} + y_{jk} \geq 1$). Finally, the continuous variable z_k represents the maximum value of y_{jk} across all containers for dimension k . The objective function minimizes a weighted sum of these maximum imbalance measures across all dimensions.

B.2.4 Workload Appointment

The WA problem simulates the allocation of workloads (such as data stream processing tasks) to the minimum number of workers (such as servers). A core requirement is allocation robustness: the entire system must continue functioning normally even if any single worker fails. No tasks should be lost. This is typically achieved through redundancy, such as ensuring each task can be handled by multiple workers. The problem is modelled as a packing problem with allocation constraints. Given the task set M , the worker set N , and the subset N_i of workers capable of handling task i , the standard MILP formulation of WA is as follows:

$$\begin{aligned} \min_{x,y} \quad & \sum_{j \in N} y_j \\ \text{s.t.} \quad & x_{ij} \leq a_i y_j \quad \forall i \in M, \forall j \in N^i \\ & \sum_{i \in M: j \in N^i} x_{ij} \leq b_j \quad \forall j \in N \\ & \sum_{j \in N^i \setminus \{j'\}} x_{ij} \geq a_i \quad \forall i \in M, \forall j' \in N^i \\ & y_j \in \{0, 1\} \quad \forall j \in N \\ & 0 \leq x_{ij} \leq b_j \quad \forall i \in M, \forall j \in N^i \end{aligned}$$

The binary variable $y_j \in \{0, 1\}$ indicates whether worker j is activated (1 for yes, 0 for no). The continuous variable x_{ij} denotes the proportion of task i allocated to worker j . a_i represents the load size of task i , while b_j denotes the capacity of worker j .

B.3 Solving State-Level Prediction

This section introduces the benchmark problems for solving state-level prediction tasks, including Set Covering (SC), Combinatorial Auctions (CA), Capacitated Facility Location with Unsplittable Demand (CFL), and Maximum Independent Set (MIS). The description of CA and MIS are the same as in the element-level prediction tasks, while the introduction of SC [56] and CFL [57] are given below.

B.3.1 Set Covering

In the SC problem, given m elements and n sets of elements, we aim to cover all elements using as few sets as possible. The union of n sets forms a collection S covering m elements, each of which belongs to at least one set. The SC problem can be formulated as follows [56]:

$$\begin{aligned}
& \min \sum_{i=1}^n x_i \\
\text{s.t. } & \sum_{i:j \in s_i} x_i \geq 1, \quad j = 1, \dots, m \\
& x_i \in \{0, 1\}, \quad i = 1, \dots, n
\end{aligned}$$

where x_i denotes whether the i -th set s_i is selected. For the SC problem, we train and test on instances with $m = 400, n = 750$, and transfer on instances with $m = 500, n = 1000$.

B.3.2 Combinatorial Auctions

In this part of experiments, we train and test on instances with $m = 100$ items and $n = 500$ bids, and the transfer experiment is on instances with $m = 200$ items and $n = 1000$ bids.

B.3.3 Capacitated Facility Location with Unsplittable Demand

In the CFL problem, given n customers with demand $\{d_j\}_{j=1}^n$ and m facilities with fixed operating costs $\{f_i\}_{i=1}^m$ and capacity $\{s_i\}_{i=1}^m$, let c_{ij}/d_j be the unit transportation cost between facility i and customer j , and p_{ij}/d_j be the unit profit generated by facility i supplying customer j . The CFL problem is formulated as follows [57]:

$$\begin{aligned}
& \min \sum_{i=1}^m \sum_{j=1}^n c_{ij} x_{ij} + \sum_{i=1}^m f_i y_i \\
\text{subject to } & \sum_{j=1}^n d_j x_{ij} \leq s_i y_i, \quad i = 1, \dots, m \\
& \sum_{i=1}^m x_{ij} \geq 1, \quad j = 1, \dots, n \\
& x_{ij} \in \{0, 1\} \quad \forall i, j \\
& y_i \in \{0, 1\} \quad \forall i
\end{aligned}$$

where each variable x_{ij} denotes the decision of facility i to meet the demand of customer j , while each variable y_i denotes the decision of facility i to develop and operate. For the CFL problem, we train and test on instances with $n = 35, m = 35$, and transfer on instances with $n = 60, m = 35$.

Appendix C Primal Gap and Primal Integral

Here we give the definition of the Primal Gap (PG) and Primal Integral (PI) metrics following [50]. PG is used to measure the relative distance between a feasible solution $\tilde{\mathbf{x}}$ and the objective value of the best known solution \mathbf{x}^* , i.e., the best known objective

value (BKV). It is a scalar value ranging between [0,1], where a smaller value indicates the solution is closer to optimal. PG is defined as:

$$PG(\tilde{\mathbf{x}}) = \begin{cases} 0, & \text{if } |c^\top \tilde{\mathbf{x}}| = |c^\top \mathbf{x}^*| = 0, \\ 1, & \text{if } c^\top \mathbf{x}^* \cdot c^\top \tilde{\mathbf{x}} < 0, \\ \frac{|c^\top \mathbf{x}^* - c^\top \tilde{\mathbf{x}}|}{\max\{|c^\top \mathbf{x}^*|, |c^\top \tilde{\mathbf{x}}|\}}, & \text{else.} \end{cases}$$

Note that for two feasible MILP solutions $\tilde{\mathbf{x}}_1$ and $\tilde{\mathbf{x}}_2$, if $c^\top \tilde{\mathbf{x}}_1 < c^\top \tilde{\mathbf{x}}_2$ and $\text{sgn}(c^\top \tilde{\mathbf{x}}_1) = \text{sgn}(c^\top \tilde{\mathbf{x}}_2)$, then $PG(\tilde{\mathbf{x}}_1) < PG(\tilde{\mathbf{x}}_2)$ holds.

Based on PG, we can define a time-varying PG function $p(t)$ as:

$$p(t) = \begin{cases} 1, & \text{if no incumbent found by time } t \\ PG(\tilde{\mathbf{x}}(t)), & \text{with } \tilde{\mathbf{x}}(t) \text{ being the incumbent at time } t \end{cases}$$

which enables us to define PI as the integral of the PG function $p(t)$ over the whole solving time T , serving to measure the cumulative performance of the entire solving process in terms of solution quality. It reflects the relationship between obtaining high-quality solutions and time expenditure, with lower values indicating higher efficiency of the solving process [50]. Specifically, PI is defined as follows:

$$PI(T) = \int_{t=0}^T p(t)dt = \sum_{i=1}^I p(t_{i-1}) \cdot (t_i - t_{i-1})$$

where t_i denotes the time at which the i -th solution is found with $t_0 = 0$, $t_I = T$.

Appendix D Implementation Details

D.1 Hyperparameters of Model Training

As mentioned in Section 4, throughout the experiments, we use the same neural architecture for both BGNN (2 layers) and our method (4 layers and 2 heads) to extract 64 dimensional features for both variables and constraints. Other training-related hyperparameters are reported in Table D4.

D.2 Hyperparameters of Predict-and-Search Frameworks

For predict-and-search experiments in Section 4.2, the search-related hyperparameters fine-tuned for each method and dataset are listed in Table D5 and D6. Within the PaS framework, enhanced prediction accuracy enables us to confidently fix a greater number of parameters to achieve superior results. Conversely, under the Apollo framework, where parameter fixing is required to correct actual prediction outcomes, we employ identical parameters to BGNN.

Table D4: Hyperparameters of the BGNN and our neural architecture for different tasks

| Task | Model | Batch size | Learning rate | Epochs |
|------------------------------------|-------|------------|---------------|--------|
| Feasibility prediction | BGNN | 64 | 3e-4 | 10000 |
| | Ours | 64 | 8e-4 | 10000 |
| Optimal objective value prediction | BGNN | 64 | 3e-4 | 12000 |
| | Ours | 64 | 8e-4 | 12000 |
| Binary variable prediction | BGNN | 64 | 3e-3 | 100 |
| | Ours | 64 | 8e-4 | 100 |
| Branching strategy learning | BGNN | 64 | 1e-3 | 1000 |
| | Ours | 64 | 1e-3 | 1000 |

Table D5: Hyperparameters of the PaS framework

| Dataset | PaS-BGNN | | | PaS-Ours | | |
|---------|----------|-------|----------|----------|-------|----------|
| | k_0 | k_1 | Δ | k_0 | k_1 | Δ |
| IP | 400 | 5 | 40 | 400 | 5 | 40 |
| WA | 0 | 500 | 40 | 0 | 500 | 40 |
| MIS | 300 | 300 | 40 | 400 | 400 | 40 |
| CA | 40 | 0 | 40 | 50 | 0 | 40 |

Table D6: Hyperparameters of the Apollo framework (values within each parentheses is the combination $(k_0^{(i)}, k_1^{(i)}, \Delta^{(i)})$ of iteration i)

| Iteration | Dataset | | | |
|-----------|-------------|------------|------------|------------|
| | IP | WA | MIS | CA |
| 1 | (100,20,50) | (60,600,5) | (50,50,50) | (100,0,60) |
| 2 | (40,15,20) | (50,500,5) | (40,15,40) | (50,0,50) |
| 3 | (20,15,10) | (40,400,5) | (20,15,30) | (40,0,40) |
| 4 | (5,50,30) | (30,0,5) | (1,5,10) | (30,0,30) |

D.3 Implementation Environment

Our model was implemented using PyTorch 2.4.1 and trained on an Ubuntu 20.04.6 LTS system equipped with an Intel(R) Core(TM) i9-10920X CPU operating at 3.5GHz, 128GB of memory, and an NVIDIA GeForce RTX 4090 GPU.

Appendix E Excluded MIPLIB Instances

In the MIPLIB experiments, 25 out of the 240 MIPLIB instances are excluded due to three reasons: 1) no binary variables after preprocessing, 2) no feasible solution found after 3,600 seconds Gurobi solving, and 3) out-of-memory. The specific excluded instances are listed in Table E7. All the remaining 215 MIPLIB instances are used in our experiments, among which the largest problem contains 550,539 variables, 1,484 constraints and 1,101,078 nonzeros.

Table E7: Excluded MILPLIB instances

| Issue | Instance name |
|--|---|
| No binary variable after presolving (12 instances) | buildingenergy, ex9, ex10, enlight_hard, gen-ip002, gen-ip054, n5-3, neos-3024952-loue, neos-3083819-nubu, ns1952667, supportcase12, supportcase42 |
| No feasible solution after 3,600 seconds Gurobi solving (10 instances) | supportcase19, bnatt500, cryptanalysiskb128n5obj14, cryptanalysiskb128n5obj16, fhnw-binpack4-4, neos-2075418-temuka, neos-3988577-wolgan, neos859080, rail02, supportcase22 |
| Out-of-memory (3 instances) | square47, neos-3402454-bohle, neos-5114902-kasavu |

References

- [1] Kalinin, K.P., Gladrow, J., Chu, J., Clegg, J.H., Cletheroe, D., Kelly, D.J., Rahmani, B., Brennan, G., Canakci, B., Falck, F., *et al.*: Analog optical computer for ai inference and combinatorial optimization. *Nature* **645**, 354–361 (2025)
- [2] Romera-Paredes, B., Barekatain, M., Novikov, A., Balog, M., Kumar, M.P., Dupont, E., Ruiz, F.J., Ellenberg, J.S., Wang, P., Fawzi, O., *et al.*: Mathematical discoveries from program search with large language models. *Nature* **625**(7995), 468–475 (2024)
- [3] Du, Y., Jamasb, A.R., Guo, J., Fu, T., Harris, C., Wang, Y., Duan, C., Liò, P., Schwaller, P., Blundell, T.L.: Machine learning-aided generative molecular design. *Nature Machine Intelligence* **6**(6), 589–604 (2024)
- [4] Naseri, G., Koffas, M.A.: Application of combinatorial optimization strategies in synthetic biology. *Nature Communications* **11**(1), 2446 (2020)
- [5] Mirhoseini, A., Goldie, A., Yazgan, M., Jiang, J.W., Songhor, E., Wang, S., Lee, Y.-J., Johnson, E., Pathak, O., Nova, A., *et al.*: A graph placement methodology for fast chip design. *Nature* **594**(7862), 207–212 (2021)

- [6] Bengio, Y., Lodi, A., Prouvost, A.: Machine learning for combinatorial optimization: a methodological tour d'horizon. *European Journal of Operational Research* **290**(2), 405–421 (2021)
- [7] Li, S., Kulkarni, J., Menache, I., Wu, C., Li, B.: Towards foundation models for mixed integer linear programming. In: The Thirteenth International Conference on Learning Representations (2025)
- [8] Naderi, B., Ruiz, R., Roshanaei, V.: Mixed-integer programming vs. constraint programming for shop scheduling problems: new results and outlook. *INFORMS Journal on Computing* **35**(4), 817–843 (2023)
- [9] Zhou, H., Qin, H., Cheng, C., Rousseau, L.-M.: An exact algorithm for the two-echelon vehicle routing problem with drones. *Transportation research part B: Methodological* **168**, 124–150 (2023)
- [10] Ararat, Ç., Meimanjan, N.: Computation of systemic risk measures: a mixed-integer programming approach. *Operations Research* **71**(6), 2130–2145 (2023)
- [11] Poos, A.M., Maicher, A., Dieckmann, A.K., Oswald, M., Eils, R., Kupiec, M., Luke, B., König, R.: Mixed integer linear programming based machine learning approach identifies regulators of telomerase in yeast. *Nucleic Acids Research* **44**(10), 93–93 (2016)
- [12] Maragno, D., Wiberg, H., Bertsimas, D., Birbil, S.İ., Hertog, D., Fajemisin, A.O.: Mixed-integer optimization with constraint learning. *Operations Research* **73**(2), 1011–1028 (2025)
- [13] McDonald, T., Tsay, C., Schweidtmann, A.M., Yorke-Smith, N.: Mixed-integer optimisation of graph neural networks for computer-aided molecular design. *Computers & Chemical Engineering* **185**, 108660 (2024)
- [14] Clautiaux, F., Ljubic, I.: Last fifty years of integer linear programming: A focus on recent practical advances. *European Journal of Operational Research* **324**(3), 707–731 (2025)
- [15] Scavuzzo, L., Aardal, K., Lodi, A., Yorke-Smith, N.: Machine learning augmented branch and bound for mixed integer linear programming. *Mathematical Programming*, 1–44 (2024)
- [16] Ding, J.-Y., Zhang, C., Shen, L., Li, S., Wang, B., Xu, Y., Song, L.: Accelerating primal solution findings for mixed integer programs based on solution prediction. In: Proceedings of the AAAI Conference on Artificial Intelligence, vol. 34, pp. 1452–1459 (2020)
- [17] Nair, V., Bartunov, S., Gimeno, F., Von Glehn, I., Lichocki, P., Lobov, I., O'Donoghue, B., Sonnerat, N., Tjandraatmadja, C., Wang, P., et al.: Solving

mixed integer programs using neural networks. arXiv preprint arXiv:2012.13349 (2020)

[18] Khalil, E.B., Morris, C., Lodi, A.: Mip-gnn: A data-driven framework for guiding combinatorial solvers. In: Proceedings of the AAAI Conference on Artificial Intelligence, vol. 36, pp. 10219–10227 (2022)

[19] Han, Q., Yang, L., Chen, Q., Zhou, X., Zhang, D., Wang, A., Sun, R., Luo, X.: A gnn-guided predict-and-search framework for mixed-integer linear programming. In: The Eleventh International Conference on Learning Representations (2023)

[20] Huang, T., Ferber, A.M., Zharmagambetov, A., Tian, Y., Dilkina, B.: Contrastive predict-and-search for mixed integer linear programs. In: International Conference on Machine Learning, pp. 19757–19771 (2024). PMLR

[21] Liu, H., Wang, J., Geng, Z., Li, X., Zong, Y., Zhu, F., Hao, J., Wu, F.: Apollo-milp: An alternating prediction-correction neural solving framework for mixed-integer linear programming. In: The Thirteenth International Conference on Learning Representations (2025)

[22] Song, J., Yue, Y., Dilkina, B., *et al.*: A general large neighborhood search framework for solving integer linear programs. Advances in Neural Information Processing Systems **33**, 20012–20023 (2020)

[23] Wu, Y., Song, W., Cao, Z., Zhang, J.: Learning large neighborhood search policy for integer programming. Advances in Neural Information Processing Systems **34**, 30075–30087 (2021)

[24] Huang, T., Ferber, A.M., Tian, Y., Dilkina, B., Steiner, B.: Searching large neighborhoods for integer linear programs with contrastive learning. In: International Conference on Machine Learning, pp. 13869–13890 (2023). PMLR

[25] Gasse, M., Chételat, D., Ferroni, N., Charlin, L., Lodi, A.: Exact combinatorial optimization with graph convolutional neural networks. Advances in neural information processing systems **32**, 15580–15592 (2019)

[26] Gupta, P., Gasse, M., Khalil, E., Mudigonda, P., Lodi, A., Bengio, Y.: Hybrid models for learning to branch. Advances in Neural Information Processing Systems **33**, 18087–18097 (2020)

[27] Zarpellon, G., Jo, J., Lodi, A., Bengio, Y.: Parameterizing branch-and-bound search trees to learn branching policies. In: Proceedings of the AAAI Conference on Artificial Intelligence, vol. 35, pp. 3931–3939 (2021)

[28] Gupta, P., Khalil, E.B., Chételat, D., Gasse, M., Lodi, A., Bengio, Y., Kumar, M.P.: Lookback for learning to branch. Transactions on Machine Learning Research (2022)

[29] Scavuzzo, L., Chen, F., Chételat, D., Gasse, M., Lodi, A., Yorke-Smith, N., Aardal, K.: Learning to branch with tree mdps. *Advances in Neural Information Processing Systems* **35**, 18514–18526 (2022)

[30] Zhang, C., Ouyang, W., Yuan, H., Gong, L., Sun, Y., Guo, Z., Dong, Z., Yan, J.: Towards imitation learning to branch for mip: A hybrid reinforcement learning based sample augmentation approach. In: *The Twelfth International Conference on Learning Representations* (2024)

[31] Sun, Y., Wang, K., Hu, Z., Wu, R., Wu, Y., Song, W., Shen, X., Lv, T., Fan, C.: Mgmacth: Fast matchmaking with nonlinear objective and constraints via multimodal deep graph learning. In: *Proceedings of the 30th ACM SIGKDD Conference on Knowledge Discovery and Data Mining*, pp. 5741–5751 (2024)

[32] Feng, S., Yang, Y.: Sorrel: Suboptimal-demonstration-guided reinforcement learning for learning to branch. In: *Proceedings of the AAAI Conference on Artificial Intelligence*, vol. 39, pp. 11212–11220 (2025)

[33] Tang, Y., Agrawal, S., Faenza, Y.: Reinforcement learning for integer programming: Learning to cut. In: *International Conference on Machine Learning*, pp. 9367–9376 (2020). PMLR

[34] Wang, J., Wang, Z., Li, X., Kuang, Y., Shi, Z., Zhu, F., Yuan, M., Zeng, J., Zhang, Y., Wu, F.: Learning to cut via hierarchical sequence/set model for efficient mixed-integer programming. *IEEE Transactions on Pattern Analysis and Machine Intelligence* **46**(12), 9697–9713 (2024)

[35] Paulus, M.B., Zarpellon, G., Krause, A., Charlin, L., Maddison, C.: Learning to cut by looking ahead: Cutting plane selection via imitation learning. In: *International Conference on Machine Learning*, pp. 17584–17600 (2022). PMLR

[36] Ling, H., Wang, Z., Wang, J.: Learning to stop cut generation for efficient mixed-integer linear programming. In: *Proceedings of the AAAI Conference on Artificial Intelligence*, vol. 38, pp. 20759–20767 (2024)

[37] Puigdemont, P., Skoulakis, S., Chrysos, G., Cevher, V.: Learning to remove cuts in integer linear programming. In: *International Conference on Machine Learning*, pp. 41235–41255 (2024). PMLR

[38] Cappart, Q., Chételat, D., Khalil, E.B., Lodi, A., Morris, C., Veličković, P.: Combinatorial optimization and reasoning with graph neural networks. *Journal of Machine Learning Research* **24**(130), 1–61 (2023)

[39] Li, Q., Han, Z., Wu, X.-M.: Deeper insights into graph convolutional networks for semi-supervised learning. In: *Proceedings of the AAAI Conference on Artificial Intelligence*, vol. 32 (2018)

[40] Topping, J., Di Giovanni, F., Chamberlain, B.P., Dong, X., Bronstein, M.M.: Understanding over-squashing and bottlenecks on graphs via curvature. In: International Conference on Learning Representations (2022)

[41] Chen, Z., Liu, J., Wang, X., Lu, J., Yin, W.: On representing mixed-integer linear programs by graph neural networks. In: International Conference on Learning Representations (2023)

[42] Chen, Z., Liu, J., Chen, X., Wang, W., Yin, W.: Rethinking the capacity of graph neural networks for branching strategy. Advances in Neural Information Processing Systems **37**, 123991–124024 (2024)

[43] Chen, Z., Chen, X., Liu, J., Wang, X., Yin, W.: Expressive power of graph neural networks for (mixed-integer) quadratic programs. In: Forty-second International Conference on Machine Learning (2025)

[44] Vaswani, A., Shazeer, N., Parmar, N., Uszkoreit, J., Jones, L., Gomez, A.N., Kaiser, L., Polosukhin, I.: Attention is all you need. Advances in Neural Information Processing Systems **30**, 6000–6010 (2017)

[45] Deng, C., Yue, Z., Zhang, Z.: Polynormer: Polynomial-expressive graph transformer in linear time. In: The Twelfth International Conference on Learning Representations (2024)

[46] Bolusani, S., Besançon, M., Bestuzheva, K., Chmiela, A., Dionísio, J., Donkiewicz, T., Doornmalen, J., Eifler, L., Ghannam, M., Gleixner, A., Graczyk, C., Halbig, K., Hettke, I., Hoen, A., Hojny, C., Hulst, R., Kamp, D., Koch, T., Kofler, K., Lentz, J., Manns, J., Mexi, G., Mühmer, E., Pfetsch, M.E., Schlässer, F., Serrano, F., Shinano, Y., Turner, M., Vigerske, S., Weninger, D., Xu, L.: The SCIP Optimization Suite 9.0. Technical report, Optimization Online (February 2024). <https://optimization-online.org/2024/02/the-scip-optimization-suite-9-0/>

[47] Gasse, M., Bowly, S., Cappart, Q., Charfreitag, J., Charlin, L., Chételat, D., Chmiela, A., Dumouchelle, J., Gleixner, A., Kazachkov, A.M., *et al.*: The machine learning for combinatorial optimization competition (ml4co): Results and insights. In: NeurIPS 2021 Competitions and Demonstrations Track, pp. 220–231 (2022). PMLR

[48] Prouvost, A., Dumouchelle, J., Scavuzzo, L., Gasse, M., Chételat, D., Lodi, A.: Ecole: A gym-like library for machine learning in combinatorial optimization solvers. In: Learning Meets Combinatorial Algorithms at NeurIPS2020 (2020)

[49] LLC Gurobi Optimization: Gurobi Optimizer (2021). <https://www.gurobi.com>

[50] Berthold, T.: Measuring the impact of primal heuristics. Operations Research Letters **41**(6), 611–614 (2013)

- [51] Ancona, M., Ceolini, E., Öztireli, C., Gross, M.: Towards better understanding of gradient-based attribution methods for deep neural networks. In: International Conference on Learning Representations (2018)
- [52] Brody, S., Alon, U., Yahav, E.: How attentive are graph attention networks? In: International Conference on Learning Representations (2022)
- [53] Gleixner, A., Hendel, G., Gamrath, G., Achterberg, T., Bastubbe, M., Berthold, T., Christophel, P., Jarck, K., Koch, T., Linderoth, J., *et al.*: Miplib 2017: data-driven compilation of the 6th mixed-integer programming library. Mathematical Programming Computation **13**(3), 443–490 (2021)
- [54] Bergman, D., Cire, A.A., Van Hoeve, W.-J., Hooker, J.: Decision Diagrams for Optimization vol. 1. Springer, Berlin, Heidelberg (2016)
- [55] Leyton-Brown, K., Pearson, M., Shoham, Y.: Towards a universal test suite for combinatorial auction algorithms. In: Proceedings of the 2nd ACM Conference on Electronic Commerce, pp. 66–76 (2000)
- [56] Balas, E., Ho, A.: Set covering algorithms using cutting planes, heuristics, and subgradient optimization: a computational study. In: Padberg, M.W. (ed.) Combinatorial Optimization, pp. 37–60. Springer, Berlin, Heidelberg (2009)
- [57] Cornu  jols, G., Sridharan, R., Thizy, J.-M.: A comparison of heuristics and relaxations for the capacitated plant location problem. European Journal of Operational Research **50**(3), 280–297 (1991)